Ferroxidase Kinetics of Human Liver Apoferritin, Recombinant H-Chain Apoferritin, and Site-Directed Mutants†

Shujun Sun,‡ Paolo Arosio,*,§ Sonia Levi,§ and N. Dennis Chasteen*,‡

Department of Chemistry, University of New Hampshire, Durham, New Hampshire 03824, and Department of Biomedical Science and Technology, DIBIT, Institute San Raffaele, University of Milano, Via Olgettina 60, 20132 Milano, Italy

Received March 19, 1993; Revised Manuscript Received June 18, 1993®

ABSTRACT: A detailed study of the kinetics of iron(II) oxidation by molecular oxygen in natural and recombinant human apoferritins has been carried out using electrode oximetry to better understand the ferroxidase activity of the protein shell. A comparative study of recombinant L-chain ferritin (rLF), recombinant H-chain ferritin (rHF), and variants has shown that (1) rLF lacks a ferroxidase activity, confirming the results of previous studies; (2) the ferroxidase site of rHF involves Glu-62 and His-65, presumably as Fe^{2+} ligands, since mutation of these residues abolishes most of the oxidase activity, in agreement with previous studies; and (3) mutation of both the putative ferroxidase and nucleation site ligands in rHF renders the protein totally incapable of catalyzing the oxidation of Fe^{2+} whereas mutation of nucleation site ligands alone (Glu-61, Glu-64, and Glu-67) decreases the activity only slightly. Analysis of the kinetics of rHF and natural human liver ferritin (HLF) (4% H-chain, 96% L-chain) gave the following apparent parameters at pH 7: $K_{m,O_2} = 6 \pm 2$ μM, $K_{m,Fe} = 80 \pm 10$ μM, and $k_{cat} = 201 \pm 14$ min^{-1} for rHF and $K_{m,O_2} = 60 \pm 12$ μM, $K_{m,Fe} = 50 \pm 10$ μM, and $k_{cat} = 31.2 \pm 0.6$ min^{-1} for HLF. Furthermore, Zn^{2+} was shown to be a noncompetitive inhibitor of Fe^{2+} oxidation in rHF but a mixed inhibitor in HLF. These different forms of Zn^{2+} inhibition in the two proteins and the higher activity of HLF than expected, based on its H-chain composition as well as differences in their enzyme kinetic parameters, suggest that H- and L-chains cooperate in modulating the ferroxidase activity of the apoferritin even though the L-subunit lacks a ferroxidase site itself.

Ferritin, the iron storage protein, is present in all eukaryotic cells. Ferritins serve to detoxify and store cellular iron in a biologically available form for use by the cell (Harrison et al., 1991; Theil, 1987, 1989). The protein shell is composed of 24 subunits of two major types, H (heavy) and L (light), designated according to small differences in their relative mobilities on SDS–PAGE[1] (Arosio et al., 1978). The subunits assemble to form a central cavity in which variable amounts of iron are deposited in a crystalline form similar to the hydrous ferric oxide mineral ferrihydrite (Harrison et al., 1991).

Ferritin can be reconstituted *in vitro* by mixing apoferritin with Fe^{2+} in the presence of molecular oxygen. Studies of horse spleen ferritin (HoSF) have shown that the protein not only functions as a reservoir for iron but also facilitates iron(II) oxidation during iron uptake by the protein (Macara et al., 1972; Bakker & Boyer, 1986; Bryce & Crichton, 1973; Bauminger et al., 1991). Recent kinetic studies have revealed that horse spleen ferritin is a true enzyme, exhibiting ferroxidase activity which is characterized by saturation kinetics with respect to the substrates Fe^{2+} and O_2 and first-order kinetics with respect to the protein (Sun & Chasteen, 1992). The protein catalyzes reaction 1, in which hydrogen peroxide is the principal product of dioxygen reduction (Xu & Chasteen, 1991).

$$2Fe^{2+} + O_2 + 4H_2O \rightarrow 2FeOOH_{core} + H_2O_2 + 4H^+ \quad (1)$$

The role of the two different subunits in iron oxidation and core formation has been the subject of considerable study. Ferritin molecules containing a large percentage of H-subunits show faster rates of iron uptake (Worwood, 1990; Wagstaff & Jacobs, 1978), while those with a large percentages of L-subunit tend to sequester more iron in their inner cavity (Artymiuk et al., 1991; Lawson et al., 1991). Site-directed mutagenesis and X-ray crystallographic studies of the Tb^{3+} derivative of recombinant H-chain apoferritin of human liver (rHF) have located a putative ferroxidase center inside the protein shell on the H-chain involving two metal binding sites, A and B, only 3 Å apart (Lawson et al., 1989, 1991). Site A involves residues Glu-27, Glu-62, His-65, and Glu-107 as ligands to Tb^{3+}, and site B involves residues Glu-61, Glu-62, and Glu-107. Residues Glu-61 and Glu-107 bridge between the two sites. Glu-27, Glu-62, and His-65 are not conserved in the L-subunit so it lacks the putative ferroxidase center. A third Tb^{3+} site (site C) composed of residues Glu-61, Glu-64, and Glu-67 is present near the ferroxidase center. This site, which is conserved in both H- and L-subunits, has been postulated to be a nucleation site for formation of the ferrihydrite mineral core (Lawson et al., 1991; Levi et al., 1992). L-Chain ferritins, while lacking the putative ferroxidase center, are capable of forming cores, albeit much slower than H-chain ferritins (Levi et al., 1989, 1992).

The previous kinetic study of the ferroxidase activity of horse spleen ferritin was unable to address the question of the role of H- and L-subunits in enzymatic activity since the protein used was a heteropolymer containing 16% H- and 84%

† This work was supported by Grant R37 GM20194 from the National Institutes of Health (N.D.C.) and by CNR Target Project Biotechnology and Bioinstrumentation Grant and CEC Bridge Grant BIOT-CT-91-0262 (P.A.).

* Authors to whom correspondence should be addressed.

‡ University of New Hampshire.

§ University of Milano.

® Abstract published in *Advance ACS Abstracts,* August 15, 1993.

[1] Abbreviations: Mes, 2-(*N*-morpholino)ethanesulfonic acid; Mops, 3-(*N*-morpholino)propanesulfonic acid; rHF, recombinant H-chain ferritin of human liver; rLF, recombinant L-chain ferritin of human liver; HLF, human liver ferritin; HoSF, horse spleen ferritin; SDS–PAGE, sodium dodecyl sulfate–polyacrylamide gel electrophoresis.

0006-2960/93/0432-9362$04.00/0

L-subunits (Sun & Chasteen, 1992). In the present work, we examine iron(II) oxidation in recombinant H-chain apoferritin and in recombinant L-chain apoferritin (rLF), both homopolymer proteins, and in human liver ferritin (HLF), which is a heteropolymer of 4% H- and 96% L-subunits. Three H-chain site-directed mutants were also studied: mutant 222, in which the two ligands Glu-62 and His-65 of the putative ferroxidase center are changed (E62K, H65G, and also K86Q); mutant A2, in which the putative nucleation site ligands Glu-61, Glu-64, and Glu-67 are changed (E61A, E64A, E67A); and mutant S1, having both the putative ferroxidase center and nucleation site ligands changed (E61A, E62K, E64A, H65G, E67A, and also D42A and K86Q) (Levi et al., 1991, 1992; Wade et al., 1991).

The rate of iron(II) oxidation was measured directly using a rapid response oxygen electrode (Sun & Chasteen, 1992) as opposed to earlier studies in which iron oxidation was measured indirectly or the color development associated with core formation was monitored [*e.g.*, Levi et al. (1988) and Wade et al. (1991)]. The electrode oximetry measurements enable us to carry out a detailed kinetic study and analysis of the iron oxidation reaction in apoferritin and site-directed mutants which has not been previously possible.

The results further delineate the role of the H- and L-subunits in the oxidation of Fe^{2+}. The experiments show that the ferroxidase activity of human liver ferritin originates from the catalytic active site on the H-subunit and that the mutation of the putative nucleation site has little effect on the rate of Fe^{2+} oxidation. Recombinant L-chain ferritin is shown to have virtually no ferroxidase activity itself; however, the L-subunit significantly modulates the ferroxidase activity of the protein in mixed L-chain, H-chain ferritins as evidenced by changes in the nature of the inhibition of the enzyme by Zn^{2+} and by alterations in the values of the Michaelis kinetic parameters, particularly K_{m,O_2} and k_{cat}. Mixed L-chain, H-chain ferritins are more active than predicted on the basis of their H-subunit composition alone.

MATERIALS AND METHODS

All chemicals were of reagent grade and were used without further purification unless otherwise indicated. Ferrous sulfate heptahydrate was obtained from J. T. Baker Chemical Co.; Mes and Mops were purchased from Research Organics Inc.; 2,2′-dipyridyl, thioglycolic acid (TGA), and sodium acetate were from Aldrich Chemical Co., Inc.; and zinc sulfate heptahydrate was from Mallinckrodt Chemical Works. Recombinant L-chain and H-chain ferritins and H-chain variants were prepared as previously described (Levi et al., 1988) and rendered iron free by dialysis against 1% thioglycolic acid in 0.1 M sodium acetate, pH 5.5, for 24 h, followed by dialysis against 0.1 M Mops and 0.1 M NaCl, pH 7 (Levi et al., 1988). Protein concentrations were determined by Bio-Rad Coomassie brilliant blue G250 protein assay using bovine serum albumin as a standard. The H- and L-subunit composition of human liver ferritin was determined by scanning of the Coomassie blue stained SDS–PAGE gels with a densitometer (Arosio et al., 1978).

Kinetic measurements of iron(II) oxidation were performed with iron/protein ratios generally <50, where hydrogen peroxide is the main product of dioxygen reduction as given by eq 1 (Xu & Chasteen, 1991). A specially designed sample cell containing an oxygen microelectrode was used to conveniently measure the kinetics of O_2 consumption during Fe^{2+} oxidation (Sun & Chasteen, 1992). Iron(II) was added to the protein solution as freshly prepared 0.100 M $FeSO_4 \cdot 7H_2O$ in 0.05 M HCl. Reconstituted ferritin samples containing 1000 Fe/protein were prepared by gradually adding 20.8 μL of 0.100 M $FeSO_4 \cdot 7H_2O$ to 1 mL of 20.8 μM apoferritin in 0.1 M NaCl and 100 mM Mops, pH 7.10, in air over a period of 2 min. Samples were then stirred continuously for 1 h, followed by being allowed to stand overnight at 4 °C before an additional amount of Fe^{2+} solution was introduced. Zn^{2+} inhibition studies were performed by adding microliter quantities of 0.100 M $ZnSO_4 \cdot 7H_2O$ to 1 mL of 20.8 μM apoprotein, followed by incubation of the sample for 1 h at ~20 °C prior to the addition of Fe^{2+}.

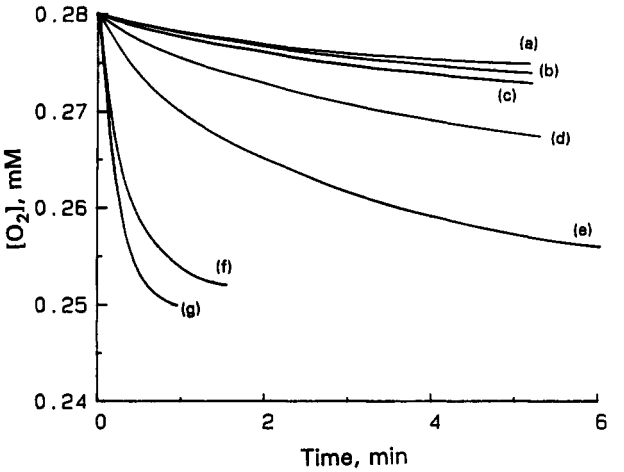

FIGURE 1: Oxygen consumption versus time for the oxidation of Fe^{2+} in (a) buffer, (b) mutant S1 (D42A, E61A, E62K, E64A, H65G, E67A, K86Q), (c) rLF, (d) mutant 222 (E62K, H65G, K86Q), (e) HLF, (f) mutant A2 (E61A, E64A, E67A), and (g) rHF. Conditions: [apoferritin] = 2.08 μM and $[Fe^{2+}]_0$ = 67 μM, in 0.1 M NaCl and 50 mM Mops, pH 7.05, 20°C.

RESULTS

Stoichiometry of Iron(II) Oxidation. Figure 1 shows the consumption of dissolved oxygen following addition of ferrous sulfate to buffer alone (curve a) and to six different apoferritins in buffer (curves b–g) using an Fe^{2+}/protein ratio of 32. From the total amount of oxygen consumed at completion of the reaction, the stoichiometry of iron(II) oxidation can be determined. The apparent stoichiometries obtained were $Fe^{2+}/O_2 = 2.1 \pm 0.1$ for rHF (curve g) and 2.7 ± 0.1 for HLF (curve e). The value of 2.1 for rHF implies that iron oxidation occurs according to reaction 1, in agreement with previous results for horse spleen apoferritin (Xu & Chasteen, 1991). The higher value of 2.7 observed for HLF is a consequence of the relatively slow rate of Fe^{2+} oxidation observed with this protein (*cf.* curves e and g) during which time some iron(II) autoxidation occurs (curve a) which has a stoichiometry of 4.0; also some of the H_2O_2 originally produced in the protein-catalyzed iron(II) oxidation reaction (eq 1) disproportionates to O_2 and H_2O via reaction 2 (Sun & Chasteen, 1992). The

$$2H_2O_2 \rightarrow O_2 + 2H_2O \qquad (2)$$

combination of autoxidation and disproportionation reactions results in an artificially high value for the stoichiometry. Therefore, the stoichiometry of 2.7 Fe^{2+} oxidized per O_2 consumed in HLF is an upper limit to the true value for the protein alone, which is probably 2.0 as for HoSF and rHF (Table I).

Ferroxidase Activity. Comparison of the curves in Figure 1 for buffer (curve a) and rHF (curve g) shows that the H-chain

Table I: Kinetic Parameters for rHF,[a] HLF,[a] and HoSF[b]

	rHF	HLF	HoSF
K_{m,O_2} (μM)	6 ± 2	60 ± 12	140 ± 30
$K_{m,Fe}$ (μM)	80 ± 10	50 ± 10	350 ± 10
k_{cat} (min^{-1})	201 ± 14	31.2 ± 0.6	80.0 ± 3.3
$K_{I,Zn}$ (μM)	74 ± 10		67 ± 11[c]
Fe^{2+}/O_2	2.1 ± 0.1	<2.7 ± 0.1	2.0 ± 0.2[d]
E_a (kJ/mol)	26.4 ± 0.1	67.3 ± 0.5	36.6 ± 1.3
ΔH^* (kJ/mol)	23.9 ± 0.1	64.8 ± 0.5	34.2 ± 1.3
ΔS^* [J/(mol·K)]	−136.0 ± 0.4	−11.0 ± 1.6	−108 ± 5

[a] Conditions: 0.1 M NaCl, 50 mM Mops, pH 7.05, 20 °C. The kinetic parameters $K_{m,Fe}$ and k_{cat} for rHF and HLF were obtained from the slopes and intercepts of the data plotted in the insets of Figure 3, and the parameter K_{m,O_2} was from the intercept of the abscissa plotted in the insets of Figure 4 using the Michaelis–Menton equation. The composition of HLF was 4% H and 96% L subunits. [b] HoSF (horse spleen apoferritin) was composed of 16% H and 84% L subunits. The data listed for HoSF were from Sun and Chasteen (1992). [c] K_I for competitive inhibition at Zn^{2+}/protein ratios ≥6. [d] From Xu and Chasteen (1991).

homopolymer greatly facilitates iron(II) oxidation whereas the L-chain homopolymer (rLF) (curve c) is virtually devoid of ferroxidase activity. Mutant 222 (E62K, H65G, K86Q) (curve d), in which the putative ferroxidase site ligands Glu-62 and His-65 have been mutated, has lost much of its ability to facilitate Fe^{2+} oxidation, a result confirming the importance of one or both of these residues in ferroxidase activity. On the other hand, mutant A2 (E61A, E64A, E67A), which is depleted of the putative nucleation site ligands Glu-61, Glu-64, and Glu-67, is nearly as active as the recombinant H-chain protein (*cf.* curves f and g), indicating that these ligands are not critical to iron(II) oxidation. Mutant S1, in which both the putative ferroxidase and nucleation sites have been mutated, is completely inactive (curve b). rLF (curve c) and mutant 222 (curve d), both lacking the ferroxidase site ligands Glu-62 and His-65, slightly accelerate the iron(II) oxidation compared to buffer and S1, suggesting that the "nucleation site" may have weak ferroxidase activity. These findings for Fe^{2+} oxidation are consistent with previous observations of the relative rates of core formation and Fe^{2+} oxidation in these proteins (Levi et al., 1988, 1989; Wade et al., 1991; Lawson et al., 1989).

To test the importance of a preexisting iron core in the iron(II) oxidation, samples of rHF and rLF were prepared containing 1000 Fe^{3+}/protein to which additional increments of Fe^{2+} were added, either 21 or 210 Fe^{2+}/protein. Figure 2 and its inset show the oxygen consumption profiles for both rHF (curve a) and rLF (curve b). When a large increment of additional Fe^{2+} is added (ΔFe^{2+}/protein = 210), iron(II) oxidation proceeded at similar rates for both rHF and rLF as shown in Figure 2. In contrast, when a small increment of Fe^{2+} is introduced (ΔFe^{2+}/protein = 21), the initial rate of oxygen consumption was about twice as large in rHF compared to rLF (0.028 *vs* 0.015 mM/min) (Figure 2, inset). These data suggest that when a large increment of iron is introduced to either H-chain or L-chain homopolymers already containing a sizable iron core (1000 Fe/protein), the surface of the mineral core itself becomes important for the oxidation of Fe^{2+}.

Enzyme Kinetics. In order to establish that HLF and rHF are true ferroxidases, measurements of the kinetics of oxygen consumption were carried out as a function of the concentrations of Fe^{2+}, O_2, and protein. Figure 3 shows the dependence of the initial rate of iron oxidation on the concentration of Fe^{2+}. Saturation kinetics with respect to Fe^{2+} is observed with both HLF and rHF (Figure 3, curve a, upper and lower panels, respectively), consistent with an enzyme catalysis mechanism in which Fe^{2+} is a substrate.

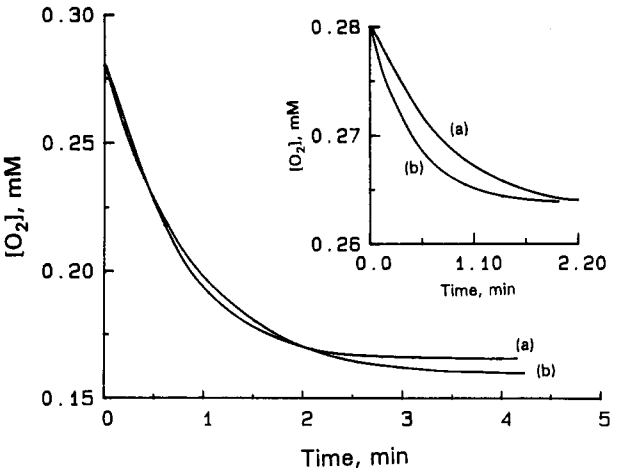

FIGURE 2: Oxygen consumption versus time for iron(II) oxidation in ferritins containing cores of 1000 Fe^{3+}. Increment of iron(II): ΔFe^{2+}/protein = 210 for Figure 2 and ΔFe^{2+}/protein = 21 for the inset. Curves: (a) rHF; (b) rLF. Conditions: [ferritin] = 2.08 μM in 0.1 M NaCl and 100 mM Mops, pH 7.10, 20 °C.

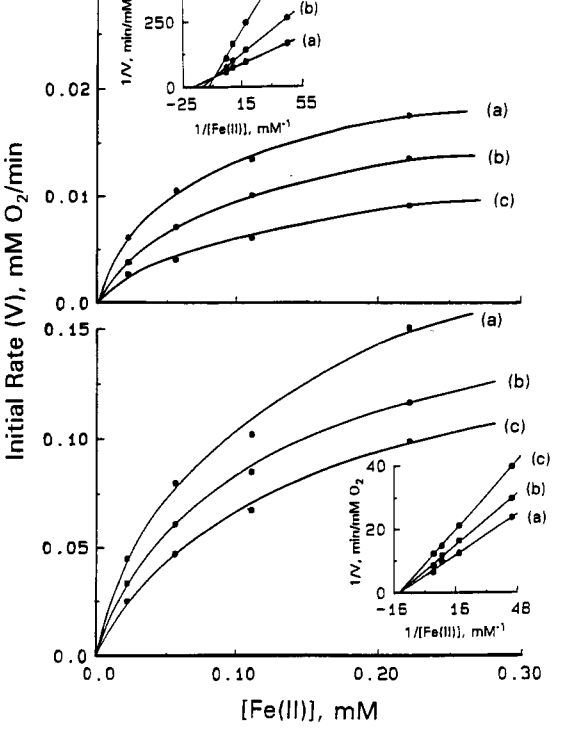

FIGURE 3: (Upper panel) Initial rate of O_2 consumption as a function of Fe^{2+} concentration in HLF at Zn^{2+}/protein = 0 (a), 6 (b), and 12 (c). (Lower panel) Initial rate of O_2 consumption as a function of iron(II) concentration in rHF at Zn^{2+}/protein = 0 (a), 12 (b), and 24 (c). Insets: Lineweaver–Burk plots with the least-squares straight lines shown. Conditions: [apoferritin] = 2.08 μM and $[O_2]_0$ = 0.28 mM in 0.1 M NaCl and 50 mM Mops, pH 7.05, 20°C.

The insets of Figure 3 illustrate the corresponding Lineweaver–Burk plots which are linear.

Figure 4 shows that saturation kinetics is also observed with respect to O_2 for HLF (upper panel) and rHF (lower panel). The rate was found to be first order with respect to protein concentration for both HLF and rHF (data not shown). The kinetic parameters from least-squares fits of the Lineweaver–Burk plots in Figures 3 and 4 are listed in Table I, along with those previously determined for horse spleen apoferritin.

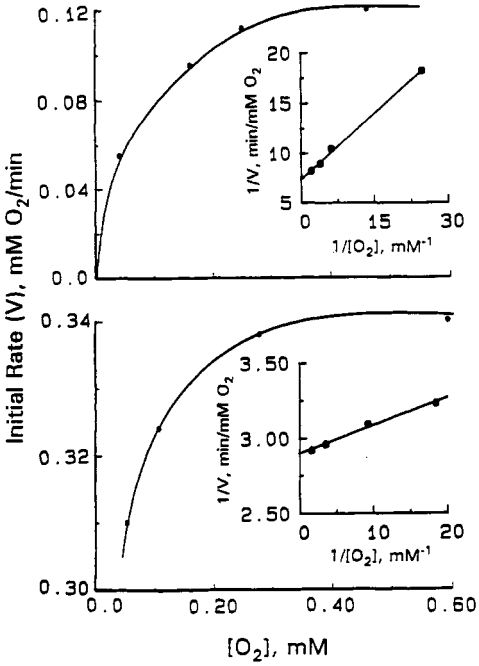

FIGURE 4: Rate of O_2 consumption as a function of O_2 concentration in rHF (upper panel) and in HLF (lower panel). Insets: double-reciprocal plots. Conditions: [apoferritin] = 10.4 μM and $[Fe^{2+}]_0$ = 440 μM in 0.1 M NaCl and 50 mM Mops, pH 7.05, 20 °C.

Zn^{2+} Inhibition. Zinc has long been known to be an inhibitor of core formation in horse spleen ferritin (Treffry et al., 1977) and has recently been shown to be a noncompetitive inhibitor of iron(II) oxidation in horse spleen apoferritin at Zn^{2+}/protein ratios ≤ 2 and a competitive inhibitor at ratios ≥ 6 (Sun & Chasteen, 1992). Zinc also inhibits iron uptake by the liver in animal studies (Matrone et al., 1975). To reveal how Zn^{2+} inhibits iron oxidation in HLF and rHF, oxygen uptake experiments were performed at various Zn^{2+}/protein ratios. The resultant Fe^{2+} saturation kinetics curves for rHF are shown in the lower panel of Figure 3, with the corresponding double-reciprocal plots presented in the inset. Noncompetitive inhibition by Zn^{2+} is clearly observed in rHF as shown by the common intercept of the abscissa (Figure 3, lower panel inset).

Two mechanisms have been previously proposed for the enzyme-catalyzed oxidation of Fe^{2+} in apoferritin; one involves oxidation of a mononuclear Fe^{2+}–protein complex (mechanism I) and the other the stepwise one-electron oxidation of a binuclear iron complex (mechanism II) (Sun & Chasteen, 1992). The two mechanisms modified to take into account zinc inhibition are given in the Appendix. As outlined there, either mechanism leads to eq 3 for noncompetitive inhibition of Fe^{2+} oxidation by Zn^{2+}, *viz.*

$$1/V = (2/P_0K_1K_2)\left(\frac{1 + [Zn^{2+}]/K_I}{\alpha[Fe^{2+}]} + \frac{(1 + [Zn^{2+}]/K_I)(1 + K_2[O_2])K_1}{\alpha}\right) \quad (3)$$

where $\alpha = (k_3 + k_3'[Zn^{2+}]/K_I)[O_2]$, $K_1 = k_1/k_{-1}$, and $K_2 = k_2/k_{-2}$. Here K_I is the inhibitor dissociation constant, and the other k's correspond to rate constants for the individual steps in the mechanism (Appendix). P_0 is the protein concentration. Thus from eq 3, plots of $1/V$ versus $1/[Fe^{2+}]$ at various fixed Zn^{2+} concentrations are expected to intercept the abscissa at the same point as is observed (Figure 3, lower panel inset). Since the rate of Fe^{2+} oxidation is much faster in the absence of inhibitor, *i.e.*, $k_3 \gg k_3'$, K_I can be obtained by plotting $1/V$ versus $[Zn^{2+}]$ at various fixed Fe^{2+} concentrations (data not shown). The intercept of the abscissa is equal to $-K_I$. A value of $K_I = 74 \pm 10$ μM is obtained (Table I).

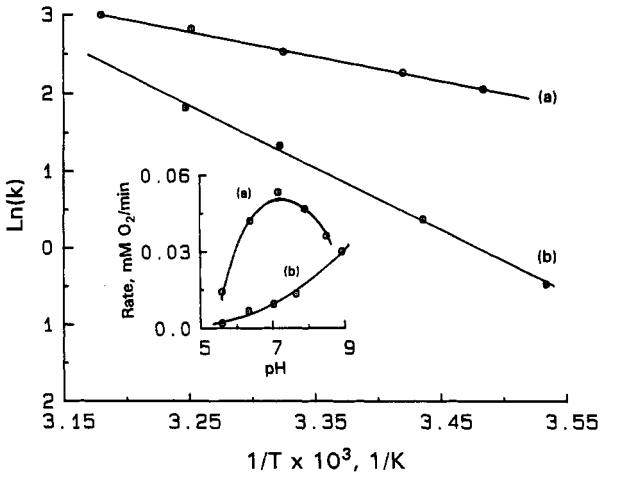

FIGURE 5: Arrhenius plot for k_1 in rHF (a) and HLF (b). Inset: pH dependence of the initial rate of O_2 incorporation in rHF (a) and HLF (b). Conditions: [apoferritin] = 4.2 μM and $[Fe^{2+}]_0$ = 110 μM in 0.1 M NaCl and 50 mM Mops, pH 7.05, for the Arrhenius plot; [apoferritin] = 2.08 μM and $[Fe^{2+}]_0$ = 67 μM in 0.1 M NaCl, 25 mM Mes, and 25 mM Mops, 20°C, for the pH profile.

In contrast to rHF, HLF shows mixed inhibition by Zn^{2+} (Figure 3, upper panel inset). Both the slope and intercept vary with Zn^{2+} concentration, but the lines intercept at a common point, namely, $1/[Fe^{2+}] \approx -4$ mM^{-1} and $1/V \approx 40$ min mM^{-1}. Unlike the noncompetitive inhibition mechanism in which the presence of inhibitor does not affect the binding of substrate, in the mixed-inhibition mechanism the enzyme and the enzyme–inhibitor complex bind substrates with different affinity (Roberts, 1977). The following Lineweaver–Burk equation is obtained for the mixed-inhibition mechanism (Appendix):

$$1/V = (2/P_0[O_2])\left(\frac{1 + [Zn^{2+}]/K_I}{(A + B[Zn^{2+}]/K_I)[Fe^{2+}]} + \frac{C + D[Zn^{2+}]/K_I}{A + B[Zn^{2+}]/K_I}\right) \quad (4)$$

where $A = k_3K_1K_2$, $B = k_3'K_1'K_2'$, $C = K_1(1 + K_2[O_2])$, and $D = (1 + K_2'[O_2])K_1'$. The intersection of Lineweaver–Burk plots at different Zn^{2+} concentrations occurs at a common point as shown in Figure 3 (upper panel inset) and is given by $1/[Fe^{2+}] = (BC - DA)/(A/K_I - B)$ and $1/V = \{(1 + 1/K_I)/(A + B)\}\{(B - DA)/(A/K_I - B)\} + (C + D)/(A + B)$. Because the slope and intercept depend on several rate and equilibrium constants, it is not possible to independently determine a value for the inhibitor constant K_I for mixed inhibition.

Temperature and pH Dependence. The Arrhenius plot of the temperature dependence of the rate constant k_1 for Fe^{2+} binding to the ferroxidase site is shown in Figure 5. The value of k_1 was obtained from the equation $V = k_1[Fe^{2+}][P_0]$ under conditions of pseudo-second-order kinetics, where the observed initial rate V is saturated with respect to O_2 concentration and undersaturated with respect to Fe^{2+} concentration. The activation energies E_a and the entropies $\Delta S^{\ddagger}$ and enthalpies $\Delta H^{\ddagger}$ of activation for rHF and HLF are summarized in Table I.

The pH dependence of the initial rate of iron oxidation is illustrated in the inset of Figure 5. A bell-shaped pH profile is observed for the oxidation reaction in rHF with a maximum rate at pH $\approx$ 7.0. Deprotonation of ferroxidase site ligands

such as His-65 is probably responsible for the observed curve as previously discussed for HoSF (Sun & Chasteen, 1992).[2] Similar curves are commonly encountered in the O_2 oxidation of small Fe^{2+} chelates [*e.g.*, Kuramura et al. (1968)]. In contrast, with HLF the initial rate of O_2 consumption increases with increasing pH (Figure 5), probably due to the low activity of the protein which is obscured by the high rate of iron(II) autoxidation at pH >7.0. The apparent stoichiometry of Fe^{2+} oxidation increases from 2.7 Fe^{2+}/O_2 at pH 7 to 3.6 at pH 8.9, close to the limiting value of 4.0 for Fe^{2+} autoxidation (eq 5).

$$4Fe^{2+} + O_2 + 6H_2O \rightleftarrows 4FeOOH_{core} + 8H^+ \quad (5)$$

DISCUSSION

Comparison of ferroxidase activity of the six different apoferritins (Figure 1) confirms that the ferroxidase site in human apoferritins is located solely on the H-subunit. A major binding site for Fe^{2+} on the L-subunit of the horse spleen protein has been identified by VO^{2+} EPR and ENDOR spectroscopy (Hanna et al., 1991), which in light of the present data is unlikely to be a ferroxidase site although it may be the initial site of Fe^{2+} binding to the protein prior to migration to the ferroxidase site.

Alteration in the postulated ferroxidase center ligands Glu-62 and His-65 (Lawson et al., 1989), which are located in the middle of the H-subunit toward the inner surface of the protein shell, does not completely eliminate the Fe^{2+} oxidation (Figure 1, curve d). Only when both the putative ferroxidase site (Glu-62 and His-65) and nucleation site (Glu-61, Glu-64, and Glu-67) ligands are mutated does the protein fail to catalyze the oxidation of iron (Figure 1, curve b). These results are consistent with the previous observation that rLF, although lacking the putative ferroxidase center, is still capable of slowly accumulating iron (Levi et al., 1989; Wade et al., 1991). Mutation of the three inner-surface glutamate residues, Glu-61, -64, and -67, of the putative nucleation site in variant A2 causes only a slight decrease in the rate of Fe^{2+} oxidation (32 Fe^{2+}/apoprotein) (Figure 1, curve f), implying that these residues, although near the ferroxidase site, have only a minor role in iron(II) oxidation under conditions of low increments of iron(II), in agreement with recent Mössbauer data (Bauminger et al., 1991). This result contrasts with that when 1000 Fe^{2+} are added to the apoprotein where the rate of core formation in mutant A2 was significantly lowered (Wade et al., 1991), an observation consistent with the postulated role for residues Glu-61, -64, and -67 in core nucleation or iron(II) oxidation at high iron loading of the protein.

The kinetic results obtained here with human liver ferritin are in accord with previous findings on horse spleen ferritin, confirming that apoferritins generally function as ferroxidases during iron uptake. The first-order kinetics with respect to Fe^{2+} concentration below levels of kinetic saturation in both rHF and HLF provide strong evidence for a mechanism involving a one-electron-transfer step during iron(II) oxidation. The μ-oxo-bridged Fe^{3+} dimers found immediately following Fe^{2+} oxidation in horse spleen ferritin (Bauminger et al., 1989) and in rHF (Bauminger et al., 1991; Treffry et al., 1992) probably are the result of iron(II) oxidation taking place in two one-electron steps by a mechanism similar to mechanism II given in the Appendix (Sun & Chasteen, 1992). The ligands of the iron dimer complex may be the same as those of the A and B sites of the Tb^{3+} dimer located at the ferroxidase center by X-ray crystallography (see introduction). Moreover, the failure of spin-trapping experiments to detect the formation of free superoxide, $O_2^{\bullet-}$ (Yu & Chasteen, 1991; Grady et al., 1989), can be accounted for by mechanism II since the O_2^{-} produced upon oxidation of the first Fe^{2+} remains bound, forming a Fe^{3+}–$O_2^{\bullet-}$ protein complex. Thus, mechanism II is in better accord with all available kinetic and spectroscopic data than is mechanism I.

The k_{cat} values for the various ferritins follow the order rHF (201 min^{-1}) > HoSF (80 min^{-1}) > HLF (31 min^{-1}) as expected on the basis of their H-subunit content (Table I). On average, the 24-mers of rHF, HoSF, and HLF contain 24, 3.8, and 1.0 H-subunits, respectively. However when k_{cat} is expressed on a per H-subunit basis, the order of activity is reversed, *i.e.*, rHF (8.4 min^{-1} $subunit^{-1}$) < HoSF (21 min^{-1} $subunit^{-1}$) < HLF (31 min^{-1} $subunit^{-1}$). It is evident that the ferroxidase activity per H-subunit is substantially greater in the heteropolymer proteins relative to the H-chain homopolymer and appears to increase with increasing L-subunit composition. Either some of the ferroxidase sites of H-homopolymer rHF do not catalytically process the Fe^{2+} substrate and therefore do not contribute to the observed reaction rate or the presence of L-subunits in HLF and HoSF significantly enhances the catalytic activity of the ferroxidase sites that are on the H-subunits. Recent studies have shown that the L-ferritin is more efficient than H-ferritin in inducing iron mineralization possibly because it contains a higher density of negative charges in the cavity (Levi et al., 1992). Thus it is conceivable that the large ratio of nucleation to ferroxidase sites and the high nucleation efficiency of L-chains in heteropolymer proteins could enhance the turnover of Fe^{3+} produced at the ferroxidase sites, leading to the greater value of k_{cat} on a per H-subunit basis that we observe here for L-subunit rich ferritins. This finding suggests that the two chains cooperate in the mechanism of ferritin iron uptake, probably acting on different steps of the reaction pathway.

When a relatively large increment of iron(II) (≈210) is added to ferritin already containing 1000 Fe/protein, the rate of iron(II) oxidation is essentially the same for both rHF and rLF (Figure 2) even though the latter lacks a ferroxidase site (Levi et al., 1988). Under these conditions, iron(II) oxidation evidently occurs primarily on the surface of the mineral core in accord with the crystal-growth model for core formation (Macara et al., 1972, 1973). However, when a small increment of iron(II) is introduced to the protein (21 Fe^{2+}/protein) containing 1000 Fe^{3+}/protein, the initial rate of iron(II) oxidation is faster in rHF than in rLF (Figure 2, inset), presumably in this instance because of involvement of the protein ferroxidase site in Fe^{2+} oxidation in rHF. In light of the present observations and those obtained previously with HoSF (Sun & Chasteen, 1992), there are clearly at least two pathways for iron(II) oxidation in ferritin, the crystal-growth pathway involving the mineral surface (Macara et al., 1972, 1973) and the enzyme-catalysis pathway originally proposed by Crichton and Roman (1978). Oxidation of iron(II) occurs simultaneously by both pathways, but each predominates under different circumstances depending on the size of the ferritin mineral core, protein subunit composition, pH, and amount of iron(II) introduced to the protein. Thus small increments of iron(II) loading favor the protein-catalysis pathway, but when this pathway becomes kinetically saturated at higher increments of iron(II), the observed rate of the reaction then

[2] The previous suggestion that hydrolysis of Fe^{2+} may be involved in the pH dependence of oxidation of Fe^{2+}–HoSF cannot be correct since the correct value of the pK_a of Fe^{2+} hydrolysis is 9.7 (Smith & Martell, 1975), not 6.5 as previously stated (Sun & Chasteen, 1992).

largely reflects the crystal-growth pathway (Sun & Chasteen, 1992).

Zinc inhibition of ferroxidase activity of the ferritins is complex. It is noncompetitive for rHF (Figure 3, lower panel) and for HoSF at low Zn^{2+}/protein ratios ≤2 but becomes competitive at ratios ≥6 (Sun & Chasteen, 1992). Mixed inhibition is observed in HLF at ratios ≤12 (Figure 3, upper panel) and competitive inhibition at ratios >24 (data not shown). Four kinds of Zn^{2+} binding sites have been located inside the cavity and in the 3-fold channels of the L-chain of horse spleen ferritin by X-ray crystallography (Harrison et al., 1986), but the number and location of Zn^{2+} binding sites on H-chain ferritin are unknown. The recent proposal that Zn^{2+} inhibition at a high Zn^{2+}/protein ratio of 240:1 in horse and sheep spleen apoferritin occurs from Zn^{2+} binding in the 3-fold channels (Yablonski & Theil, 1992) is at variance with recent site-directed mutagenesis studies of rHF showing that Zn^{2+} inhibition is retained when the 3-fold channels are mutated (Treffry et al., 1993). Since the rate of Fe^{2+} oxidation in mutant A2, which lacks the putative "C" nucleation site ligands Glu-61, -64, and -67, is nearly the same as that of the wild type, our data indicate that this site is unlikely a key binding site for zinc inhibition. Thus the observed noncompetitive inhibition in rHF and HoSF and the mixed competitive/noncompetitive inhibition in HLF appear to involve zinc binding sites yet to be identified. Since Zn^{2+} inhibition gradually becomes competitive at higher ratios in both HLF and HoSF, it is evident that Zn^{2+} at sufficiently high concentration ultimately can compete directly with Fe^{2+} for binding at the H-chain ferroxidase sites in these proteins.

The K_I (=74 μM) for noncompetitive inhibition in rHF is very similar to the value of 67 μM (Zn^{2+}/protein ≥ 6) for competitive inhibition in HoSF (Table I). The similarity in inhibition constants suggests similar ligands for Zn^{2+} in both instances. The formation constant ($1/K_I \sim 10^4\ M^{-1}$) for the Zn^{2+}–protein complex is typical of the values commonly observed for small chelates having two to three coordinating carboxylate groups (Martell & Smith, 1977), a result consistent with the makeup of crystallographically identified Zn^{2+} sites of HoSF which involve aspartate and glutamate residues (Harrison et al., 1986).

The observed dioxygen saturation kinetics (Figure 4) shows that kinetic saturation is achieved at lower concentrations of O_2 in rHF compared with HLF, indicative of an apparent tighter oxygen binding to Fe^{2+}-rHF than to Fe^{2+}-HLF. The K_{m,O_2} for rHF is about 10 times smaller than that of HLF (Table I) and suggests that the L-subunit modulates the affinity of the Fe^{2+}–protein complex for O_2 in the heteropolymer.

The small activation energy (E_a = 26 kJ) for k_1, the rate constant for Fe^{2+} binding to the ferroxidase site in rHF, is consistent with the high ferroxidase activity of the protein compared to HLF (Table I). The large negative entropy of activation [$\Delta S^{\ddagger} = -136$ J/(mol·K)] in rHF suggests substantial changes in the protein ligand conformation upon Fe^{2+} binding, whereas the small activation entropy [$\Delta S^{\ddagger} = -11$ J/(mol·K)] in HLF is comparable to that observed upon complexation of Fe^{2+} by small chelates (Hewkin & Prince, 1970). These findings provide further evidence for the involvement of the L-subunit in modulating iron(II) oxidation in the heteropolymer. Moreover, the small negative activation entropy of HLF may account for the higher than expected reactivity of this protein based on its H-subunit composition alone.

In summary, the present data have provided further insight into the kinetic properties of the ferritins. The data demonstrate that catalytic activity is centered on the H-subunit but is clearly modulated by the presence of the L-subunit. The iron(II) oxidation kinetics of the mutants are in general accord with the rates of core formation determined in previous studies with these proteins (Levi et al., 1989; Wade et al., 1991). The kinetics observed here for both rHF and HLF are most consistent with a mechanism which may involve formation of a dimeric iron species at the ferroxidase center with iron(II) oxidation occurring via two one-electron-transfer steps involving a single dioxygen molecule as in mechanism II.

ACKNOWLEDGMENT

We thank Dr. Santambrogio for preparation of the protein samples.

APPENDIX I

Reaction Mechanisms for Noncompetitive Inhibition and Mixed Inhibition by Zn^{2+}. The previously proposed mechanisms for Fe^{2+} oxidation (Sun & Chasteen, 1992) modified to include inhibition by Zn^{2+} follow. The rate constants for the added elementary steps involving Zn^{2+} are designated by primes.

Mechanism I

Zn^{2+} binding:

$$Zn^{2+}\text{–P} \overset{K_I}{\rightleftarrows} Zn^{2+} + P \quad \text{(A1)}$$

Fe^{2+} binding:

$$Fe^{2+} + P \underset{k_{-1}}{\overset{k_1}{\rightleftarrows}} Fe^{2+}\text{–P} \quad \text{(A2)}$$

$$Fe^{2+} + Zn^{2+}\text{–P} \underset{k_{-1'}}{\overset{k_{1'}}{\rightleftarrows}} Fe^{2+}\text{–P–}Zn^{2+} \quad \text{(A3)}$$

dioxygen binding and Fe^{2+} oxidation:

$$Fe^{2+}\text{–P} + O_2 \underset{k_{-2}}{\overset{k_2}{\rightleftarrows}} Fe^{2+}(O_2)\text{–P} \overset{k_3}{\rightarrow} Fe^{3+}\text{–P} + O_2^- \quad \text{(A4)}$$

$$Fe^{2+}\text{–P–}Zn^{2+} + O_2 \underset{k_{-2'}}{\overset{k_{2'}}{\rightleftarrows}} Fe^{2+}(O_2)\text{–P–}Zn^{2+} \overset{k_{3'}}{\rightarrow} Fe^{3+}\text{–P–}Zn^{2+} + O_2^- \quad \text{(A5)}$$

iron(III) core formation:

$$Fe^{3+}\text{–P} + 2H_2O \overset{k_4}{\rightarrow} FeOOH_{core} + P + 3H^+ \quad \text{(A6)}$$

$$Fe^{3+}\text{–P–}Zn^{2+} + 2H_2O \overset{k_{4'}}{\rightarrow} FeOOH_{core} + Zn^{2+}\text{–P} + 3H^+ \quad \text{(A7)}$$

fate of superoxide:

$$2O_2^- + 2H^+ \overset{k_5}{\rightarrow} H_2O_2 + O_2 \quad \text{(A8)}$$

Mechanism II

Zn^{2+} binding:

$$Zn^{2+}\text{–P} \overset{K_I}{\rightleftarrows} Zn^{2+} + P \quad \text{(A9)}$$

Fe^{2+} binding:

$$Fe^{2+} + P \underset{k_{-1}}{\overset{k_1}{\rightleftarrows}} Fe^{2+}\text{–P} \quad \text{(A10)}$$

$$Fe^{2+} + Zn^{2+}\text{–P} \underset{k_{-1'}}{\overset{k_{1'}}{\rightleftarrows}} Zn^{2+}\text{–P–}Fe^{2+} \quad \text{(A11)}$$

dioxygen binding and first Fe^{2+} oxidation:

$$O_2 + Fe^{2+}\text{–P} \underset{k_{-2}}{\overset{k_2}{\rightleftarrows}} Fe^{2+}(O_2)P \xrightarrow{k_3} Fe^{3+}(O_2^-)P \quad \text{(A12)}$$

$$O_2 + Fe^{2+}\text{–P–}Zn^{2+} \underset{k_{-2}'}{\overset{k_2'}{\rightleftarrows}} Fe^{2+}(O_2)P\text{–}Zn^{2+} \xrightarrow{k_3'} Fe^{3+}(O_2^-)P\text{–}Zn^{2+} \quad \text{(A13)}$$

second Fe^{2+} binding/oxidation:

$$Fe^{3+}(O_2^-)P + Fe^{2+} \xrightarrow{k_4} Fe^{3+}(O_2^{2-})Fe^{3+}\text{–P} \xrightarrow{k_5, H_2O} Fe^{3+}(O^{2-})Fe^{3+}\text{–P} + H_2O_2 \quad \text{(A14)}$$

$$Fe^{3+}(O_2^-)P\text{–}Zn^{2+} + Fe^{2+} \xrightarrow{k_4'} Fe^{3+}(O_2^{2-})Fe^{3+}\text{–P–}Zn^{2+} \xrightarrow{k_5', H_2O} Fe^{3+}(O^{2-})Fe^{3+}\text{–P–}Zn^{2+} + H_2O_2 \quad \text{(A15)}$$

The steady-state approximation is used to derive the various rate equations. For example, the following expressions are combined to obtain eq 3 of the main text for mechanism I subject to the assumptions elaborated as follows:

$$d[Fe^{2+}\text{–P}]/dt = k_1[P][Fe^{2+}] - k_{-1}[Fe^{2+}\text{–P}] - k_2[O_2][Fe^{2+}\text{–P}] - k_{-2}[Fe^{2+}(O_2)P] = 0 \quad \text{(A16)}$$

$$d[Fe^{2+}\text{–P–}Zn^{2+}]/dt = k_1'[Zn^{2+}\text{–P}][Fe^{2+}] - k_{-1}'[Fe^{2+}\text{–P–}Zn^{2+}] - k_2'[Fe^{2+}\text{–P–}Zn^{2+}][O_2] + k_{-2}'[Fe^{2+}(O_2)\text{–P–}Zn^{2+}] = 0 \quad \text{(A17)}$$

$$d[Fe^{2+}(O_2)\text{–P}]/dt = k_2[Fe^{2+}\text{–P}][O_2] - (k_{-2} + k_3)[Fe^{2+}(O_2)\text{–P}] = 0 \quad \text{(A18)}$$

$$d[Fe^{2+}(O_2)\text{–P–}Zn^{2+}]/dt = k_2'[Fe^{2+}\text{–P–}Zn^{2+}][O_2] - (k_{-2}' + k_3')[Fe^{2+}(O_2)\text{–P–}Zn^{2+}] = 0 \quad \text{(A19)}$$

$$d[Fe^{3+}\text{–P}]/dt = k_3[Fe^{2+}(O_2)\text{–P}] - k_4[Fe^{3+}\text{–P}] = 0 \quad \text{(A20)}$$

$$d[Fe^{3+}\text{–P–}Zn^{2+}]/dt = k_3'[Fe^{2+}(O_2)\text{–P–}Zn^{2+}] - k_4'[Fe^{3+}\text{–P–}Zn^{2+}] = 0 \quad \text{(A21)}$$

$$d[O_2^-]/dt = k_3[Fe^{2+}(O_2)\text{–P}] + k_3'[Fe^{2+}(O_2)\text{–P–}Zn^{2+}] - 2k_5[O_2^-]^2[H^+]^2 = 0 \quad \text{(A22)}$$

The rate expression from rate-limiting eqs A4 and A5 is given by

$$V = -{}^1/_2 d[Fe^{2+}]/dt = {}^1/_2 k_3[Fe^{2+}(O_2)\text{–P}] + {}^1/_2 k_3'[Fe^{2+}(O_2)\text{–P–}Zn^{2+}] \quad \text{(A23)}$$

where $V (= d[O_2]/dt = {}^1/_2 d[Fe^{2+}]/dt)$ is the net velocity for the reaction given by eq 1 of the main text.

In deriving rate eq 3 in the main text for noncompetitive inhibition, several assumptions have been made in order to obtain a linear equation consistent with the observed data: (1) the binding of Zn^{2+} to protein does not affect the affinities of Fe^{2+} and O_2 binding to protein; *i.e.*, the equilibrium constants $K_1 = K_1'$ and $K_2 = K_2'$; (2) the rate constant of the one-electron-transfer step is reduced by Zn^{2+} binding so that $k_3' < k_3$; (3) a preequilibrium condition exists for O_2 binding in steps 4 and 5; *i.e.*, $k_3 \ll k_{-2}$ and $k_3' \ll k_{-2}'$; and (4) the one-electron-transfer reaction for oxidation of the first Fe^{3+} is rate determining (steps 4 and 5). Under these assumptions, the same double-reciprocal rate equation (eq 3, main text) is obtained for both mechanism I and mechanism II. In deriving the rate equation for mixed inhibition (eq 4, main text), the first assumption is changed such that the equilibrium constants for Fe^{2+} and O_2 binding to the protein are altered upon Zn^{2+} binding; *i.e.*, $K_1 \neq K_1'$ and $K_2 \neq K_2'$. The second through fourth assumptions are unchanged.

In the absence of Zn^{2+} inhibition and without any assumptions, a more general form of the rate equation can be derived than previously given for mechanism I (eq 8 of Sun & Chasteen, 1992), *viz.*

$$1/V = 2/P_0\left(\frac{1}{k_1[Fe^{2+}]} + \frac{k_3 + k_{-2}}{k_2k_3[O_2]} + \frac{k_{-1}(k_3 + k_{-2})}{k_1k_2[Fe^{2+}][O_2]} + \frac{1}{k_3}\right) \quad \text{(A24)}$$

When the third term is omitted, which is equivalent to assuming $k_{-1} \ll k_2[O_2]$ and $k_3 \ll k_4$ in the derivation of eq A24, the equation becomes identical to the less general form previously described (Sun & Chasteen, 1992). Equation A24 also applies to mechanism II in the absence of Zn^{2+} inhibition provided that the k_3 step in reaction A12 is assumed to be rate limiting; *i.e.*, k_4, k_5, and k_6 are larger than k_3. The previously reported eq 18 for mechanism II was derived with only the constraint that $k_2[O_2] \gg k_{-1}$ (Sun & Chasteen, 1992).

The apparent values of $K_{m,Fe}$ and K_{m,O_2} obtained from the intercept of the abscissa of the $1/V$ versus $1/[Fe^{2+}]$ and $1/V$ versus $1/[O_2]$ plots of eq A24 are given by

$$K_{m,Fe} = \frac{k_2k_3[O_2] + k_{-1}k_3(k_3 + k_{-2})}{k_1k_2[O_2] + k_1(k_3 + k_{-2})} \rightarrow \frac{k_3}{k_1} \quad \text{(A25)}$$

at saturating O_2 levels, *i.e.*, $[O_2] \rightarrow \infty$, and

$$K_{m,O_2} = \frac{(k_3 + k_{-2})k_1[Fe^{2+}] + k_{-1}k_3(k_3 + k_{-2})}{k_2k_1[Fe^{2+}] + k_3k_2} \rightarrow \frac{k_1 + k_{-2}}{k_2} \quad \text{(A26)}$$

at saturating Fe^{2+} levels, *i.e.*, $[Fe^{3+}] \rightarrow \infty$.

REFERENCES

Arosio, P., Adelman, T. G., & Drysdale, J. (1978) *J. Biol. Chem. 253*, 1056.

Artymiuk, P. J., Bauminger, E. R., Harrison, P. M., Lawson, D. M., Nowik, I., Treffry, A., &Yewdall, S. J. (1991) in *Iron Biominerals* (Frankel, R., & Blakemore, R. P., Eds.) p 269, Plenum Press, New York.

Bakker, G. R., & Boyer, R. F. (1986) *J. Biol. Chem. 261*, 13182.

Bauminger, E. R., Harrison, P. M., Nowik, I., & Treffry, A. (1989) *Biochemistry 28*, 5486.

Bauminger, E. R., Harrison, P. M., Hechel, D., Nowik, I., & Treffry, A. (1991) *Biochim. Biophys. Acta 1118*, 48.

Bryce, C. F. A., & Crichton, R. R. (1973) *Biochem. J. 133*, 301.

Crichton, R. R., & Roman, F. (1978) *J. Mol. Catal. 4*, 75.

Crichton, R. R., Roman, F., & Roland, F. (1980) *J. Inorg. Biochem. 13*, 305.

Grady, J. K., Chen, Y., Chasteen, N. D., & Harris, D. C. (1989) *J. Biol. Chem. 264*, 20224.

Hanna, P. M., Chasteen, N. D., Rottman, G. A., & Aisen, P. (1991) *Biochemistry 30*, 9210.

Harrison, P. M., Ford, G. C., Rice, D. W., Smith, J. M. A., Treffry, A., & White, J. L. (1986) in *Frontiers in Bioinorganic Chemistry* (Xavier, A., Ed.) p 268, VCH Verlagsgesellschaft, Weinheim, Germany.

Harrison, P. M., Andrews, S. C., Artymiuk, P. J., Ford, G. C., Guest, J. R., Hirzmann, J., Lawson, D. M., Livingstone, J. C., Smith, J. M. A., Treffry, A., & Yewdall, S. J. (1991) *Adv. Inorg. Chem. 36*, 449.

Hewkin, D. J., & Prince, R. H. (1970) *Coord. Chem. Rev. 5*, 45.

Lawson, D. M., Treffry, A., Artymiuk, P. J., Harrison, P. M., Yewdall, S. J., Luzzago, A., Cesareni, G., Levi, S., & Arosio, P. (1989) *FEBS Lett. 254*, 207.

Lawson, D. M., Artymiuk, P. J., Yewdall, S. J., Smith, J. M. A., Livingstone, J. C., Treffry, A., Luzzago, A., Levi, S., Arosio, P., Cesareni, G., Thomas, C. D., Shaw, W. V., & Harrison, P. M. (1991) *Nature 349*, 541.

Levi, S., Luzzago, A., Cesareni, G., Cozzi, A., Franceschinelli, F., Albertini, A., & Arosio, P. (1988) *J. Biol. Chem. 263*, 18086.

Levi, S., Salfeld, J., Franceschinelli, F., Cozzi, A., Dorner, M. H., & Arosio, P. (1989) *Biochemistry 28*, 5179.

Levi, S., Cozzi, A., Santambrogio, P., & Arosio, P. (1991) Study of the Sequences Involved in Ferritin Iron Incorporation, 10th International Conference on Iron and Iron Proteins, Oxford, U. K., July 27–31, paper O15.

Levi, S., Yewdall, S. J., Harrison, P. M., Santambrogio, P., Cozzi, A., Rovida, E., Albertini, A., & Arosio, P. (1992) *Biochem. J. 288*, 591.

Macara, I. G., Hoy, T. G., & Harrison, P. M. (1972) *Biochem. J. 126*, 151.

Macara, I. G., Hoy, T. G., & Harrison, P. M. (1973) *Biochem. J. 135*, 343.

Roberts, D. V. (1977) *Enzyme Kinetics*, pp 65 and 83, Cambridge University Press, Cambridge.

Segel, I. H. (1975) *Enzyme Kinetics*, pp 884 and 941, Wiley-Interscience, New York.

Smith, R. M., & Martell, A. E. (1976) *Critical Stability Constants*, Vol. 4, p 5, Plenum Press, New York.

Smith, R. E., & Martell, A. E. (1977) *Critical Stability Constants*, Vol. 3, pp 1–171, Plenum Press, New York.

Sun, S., & Chasteen, N. D. (1992) *J. Biol. Chem. 267*, 25160.

Theil, E. C. (1987) *Annu. Rev. Biochem. 56*, 289.

Theil, E. C. (1989) *Adv. Enzymol. Relat. Areas Mol. Biol. 63*, 421.

Treffry, A., & Harrison, P. M. (1984) *J. Inorg. Biochem. 21*, 9.

Treffry, A., Hirzmann, J., Yewdall, S. J., & Harrison, P. M. (1992) *FEBS Lett. 302*, 108.

Treffry, A., Bauminger, R., Harrision, P. M., Hechel, D., Hodson, N., & Nowik, I. (1993) Mechanism of Iron Uptake by Apoferritin Analyzed with the Aid of Zn(II) and Tb(III), 11th International Conference on Iron and Iron Proteins, Jerusaleum, Israel, May 2.

Wade, V. J., Levi, S., Arosio, P., Treffry, A., Harrison, P. M., & Mann, S. (1991) *J. Mol. Biol. 221*, 1443.

Wagstaff, M. M., & Jacobs, A. (1978) *Biochem. J. 173*, 969.

Worwood, M. (1990) *Blood Rev. 4*, 259.

Xu, B., & Chasteen, N. D. (1991) *J. Biol. Chem. 266*, 19965.

Yablonski, M. J., & Theil, E. C. (1992) *Biochemistry 31*, 9680.